The importance of details: how differences in ligand structures determine distinct functional responses in integrin $\alpha_v\beta_3$

Antonella Paladino[a], Monica Civera[b], Flavio Curnis[c], Mayra Paolillo[d], Cesare Gennari[b], Umberto Piarulli[e], Angelo Corti[c], Laura Belvisi[b] and Giorgio Colombo*[f]

[a] Dr. A. Paladino
Istituto di Chimica del Riconoscimento Molecolare CNR, via Mario Bianco 9, 20131, Milan, Italy
[b] Dr. M. Civera, Prof. C. Gennari, Prof. L. Belvisi
Università degli Studi di Milano, Dipartimento di Chimica, via Golgi 19, 20133, Milan, Italy
[c] Dr. F. Curnis, Prof. A. Corti
IRCCS Ospedale San Raffaele, Via Olgettina 60, 20132, Milan, Italy
[d] Dr. M. Paolillo
Università degli Studi di Pavia, Dipartimento di Scienze del Farmaco, Viale Taramelli 6, 27100 Pavia, Italy
[e] Prof. U. Piarulli
Università degli Studi dell'Insubria, Dipartimento di Scienza e Alta Tecnologia, Via Valleggio 11, 22100 Como (Italy)
[f] Prof. G. Colombo
Università degli Studi di Pavia, Dipartimento di Chimica, Viale Taramelli 12, 27100 Pavia, Italy
E-mail: g.colombo@unipv.it

Abstract: Ligand-based control of protein functional motions can provide novel opportunities in the study of fundamental biological mechanisms and in the development of novel therapeutics. Here, we address ligand-based modulation of integrin functions. Inhibitors of integrin $\alpha_v\beta_3$ are interesting anticancer agents but their molecular mechanisms are still unclear: peptides and peptidomimetics characterized by the RGD or isoDGR binding motifs have shown controversial agonist/antagonist effects. We investigate the differential mechanisms of integrin activation/deactivation by three distinct ligands (*cyclo*-RGDf(NMe)V (Cilengitide), *cyclo*[DKP3-RGD], *cyclo*[DKP3-isoDGR]), through comparative analysis of ligand-controlled protein internal dynamics: while RGD facilitates the onset of dynamic states leading to activation, isoDGR induces a diffuse rigidification of the complex consistent with antagonist activities. Computational predictions are experimentally probed by showing that antibody AP5, selective for active integrin conformations, binds specifically to the RGD complexes and not to the isoDGR one, supporting opposite functional roles for the two motifs targeting the same binding site.

Introduction

Integrins are heterodimeric cell adhesion receptor proteins composed of two non-covalently associated α and β subunits that contain large extracellular domains (a.k.a. ectodomains), single-pass Trans-Membrane domains, and short cytoplasmic tails. Integrins play a key role in mediating outside-in and inside-out signals across cell-membranes. Experiments have demonstrated that endogenous ligands bind the integrin ectodomain inducing conformational changes that are required for the activation of downstream intracellular signalling pathways.[1]

Several members of the integrin family (e.g. αvβ3, αvβ5, α5β1, αIIbβ3) have been shown to recognize as physiologic ligands protein domains that are characterized by the consensus tripeptidic sequence Arg-Gly-Asp (RGD). Ligand specificity is modulated both by the physical and chemical properties of the residues flanking the RGD triad and by the integrin chemical and structural features, as well as by the RGD conformation.[2]

Integrin αvβ3 overexpression is associated with the activation of signalling pathways relevant for cancer angiogenesis and other cellular pathways involved in cancer processes.[3] Hence, the protein has become a target of therapeutic interest in cancer treatment: in this context, Cilengitide,[4] a cyclic peptide presenting the RGD motif for integrin binding (compound **1** in Figure 1), has shown anti-angiogenic properties [5] turning into the first small molecule drug candidate that targets the αv subfamily of integrins. Cilengitide inhibits both αvβ3 and αvβ5, resulting in decreased cell adhesion and migration, and it has progressed to late-stage clinical trials for cancer indications. However, the results of a Phase III study in glioblastoma did not meet their primary endpoint and Cilengitide currently remains unmarketed.[6]

In general, ligand binding occurs within a crevice at the interface between α and β integrin subunits, and it is assisted by 3 metal ions located at the β3 interface; the guanidinium side chain of the RGD motif bridges the α chain via an electrostatic clamp with aspartic acids of the β-propeller domain (αv), whereas Asp carboxyl oxygens coordinate the Mn2+ ion at MIDAS (βA), and form hydrogen bonds to the β1-α1 loop of the β3 subunit. Interestingly, experimental

evidence has shown that some RGDbased cyclopeptides, including Cilengitide, do not behave as pure antagonists, but rather as partial agonists.[2a, 7] This could be one of the reasons that, at least partially, explain the failure of *cyclo*-RGDf(NMe)V (i.e. Cilengitide) in Phase III trials against glioblastoma. Recent data on endothelial cells expressing αvβ3 but adhering through β1 integrins, have shown that Cilengitide induces affinity maturation (e.g. activation) of cell surface αvβ3 leading to Src, FAK and VE-cadherin phosphorylation.[5a] However, the molecular determinants of this peculiar behavior have not been completely clarified.

In this framework, X-ray structures of integrin αvβ3 in complex with its endogenous ligand Fibronectin, FN10, in its wild-type sequence (wtFN) and a high-affinity mutant form (hFN) have helped unveil important molecular determinants of the modulation of integrin functional dynamics.[2] The complex with the wild-type physiologic ligand, wtFN, was characterized by high conformational flexibility, in particular in the integrin ectodomain. This, in turn, could favor the conformational switch of the integrin required for function.[1] In contrast, the presence of hFN determined a diffuse rigidification of the ectodomain of the receptor, which could expectedly translate in disfavoring integrin activation and in the observed antagonist character of mutated fibronectin.[2] Interestingly, dynamic changes at the local level in the binding site could be linked to the modulation of the dynamics of hinges responsible for controlling large-scale conformational transitions.

In parallel, an atomistic description of the closed-to-open transition has been detailed for the activation mechanism of αIIbβ3 integrin, based on the analysis of sequential X-ray structures.[1d] Local adjustments at the binding pocket (αIIbβ3 interface) upon ligand binding are responsible for the global structural arrangements required for function. Zhu and coworkers defined eight distinct RGD-bound conformations of the αIIbβ3 integrin headpiece obtained by soaking crystals with RGD peptides. Starting from the closed conformation, six intermediate states of the βA domain were captured between the first and last conformations. [1d] The 8th state was characterized by the swing out of the hybrid domain, driven by local changes occurring at the β1-α1 loop, α1 helix, the ADMIDAS metal and β6-α7 loop, which might prime the piston-like displacement of the α7 helix.

Modulation of integrin conformational dynamics has been investigated through the use of small molecule ligands.[8] In this context, Curnis *et al*. showed that the isoDGR motif represents an additional adhesion site for integrins that can show peculiar isoform selectivities and can perturb integrin conformational and activation properties in a different fashion from Cilengitide or other RGD-based ligands.[9] Overall, while RGD containing ligands behave as partial agonists, isoDGR integrin ligands behave as antagonists. The underlying mechanisms and their consequences on protein (de)activation have thus represented the focus of intense efforts over the last years.[8, 10] Frank and coworkers [8c] developed a library of cyclic pentapeptides containing the isoDGR motif and could rationalize their preferential isotype binding via experimental binding studies and docking simulations. An important contribution to this field is represented by the work of Ghitti and coworkers, who studied the effects of ligands on integrin αvβ3 activation by comparative Molecular Dynamics (MD) simulations of complexes with Cilengitide and two isoDGR cyclopeptides.[10] Using a cumulative simulation time of 360 ns and analyzing the trajectories via covariance and principal components analysis, they could define the main directions of motions that may be induced by the different ligands. Further investigations focusing on the isolated β3 subunit from the αvβ3 and αIIbβ3 integrins in the presence of different ligands were described by Felline *et al.*, [11] using Protein Structure Network (PSN) analysis. The results indicated that the closed and open states of the isolated β headpiece are characterized by distinct allosteric communication pathways involving conserved amino acids.

Here we focus our attention on the effects on integrin dynamics of two recently introduced synthetic ligands that have shown antagonist activities in cells, reminiscent of those displayed by high-affinity Fibronectin, hFN. The compounds, reported in Figure 1, are cyclic molecules based on a bifunctional diketopiperazine (DKP) scaffold, which, while mimicking the structural features of a cyclic peptide, represents a substantially different chemical entity. Such DKP-based ligands proved to be low-nanomolar αvβ3 ligands, with affinities comparable to Cilengitide.[12] In particular, *cyclo*[DKP3-RGD] and *cyclo*[DKP3-isoDGR] (respectively compounds **2** and **3** in Figure 1) show IC50s of 4.5 and 9 nM for αvβ3, respectively.[12-13] In human U373 glioblastoma cells, *cyclo*[DKP3-RGD] and *cyclo*[DKP3-isoDGR] showed inhibitory

effects on the FAK/Akt integrin activated transduction pathways and on integrinmediated cell infiltration process. Additionally, they induced apoptosis in glioma cells after 72h treatments.[12-13]

One important question is whether and how specific compounds with very similar binding affinities for the target induce distinct structural and dynamic perturbations, which may ultimately depend on the presence of either the RGD or isoDGR motifs, on the integrin and whether the characterization of these properties can be related to experimental tests of differential integrin activation. Indeed, considering their tight and very similar binding at the same site, it may not be obviously expected to observe a distinct modulation of integrin functionally-oriented internal dynamics and large scale motions. However, no high-resolution structure of these ligands in complex with αvβ3 has been solved yet.

To make progress in understanding the molecular effects of the small-molecules on the initial stages of the process of dynamic (de)activation of αvβ3, we can turn to computational approaches. To this end, we have carried out multi-microsecond, all-atom Molecular Dynamics (MD) simulations of the integrin αvβ3 headpiece in the presence of *cyclo*-RGDf(NMe)V (Cilengitide), *cyclo*[DKP3-RGD] and *cyclo*[DKP3-isoDGR], hereafter referred to as compound **1**, **2** and **3**, respectively. Here, we present a comparative investigation of the impact of binding different ligands on the internal dynamic properties of αvβ3. Distinct ligand-dependent dynamic traits for αvβ3, that can be correlated to the triggering or blocking of the initial steps of closed-to-open transition, emerge from the analysis. Global dynamic effects are explicitly linked to specific interaction patterns at the integrin binding site. We complete our investigation by experimentally examining the conformational effects induced by compounds **1**-**3** on αvβ3 integrin in MSR3 melanoma cells by means of the specific monoclonal antibody AP5 recognizing the active form of the β3 subunit.[14] We show that the exposure of the integrin epitope recognized by the specific antibody AP5 and the extent of AP5 binding, which report on the integrin activation state, can be correlated with the distinct dynamics states induced by the 3 ligands.

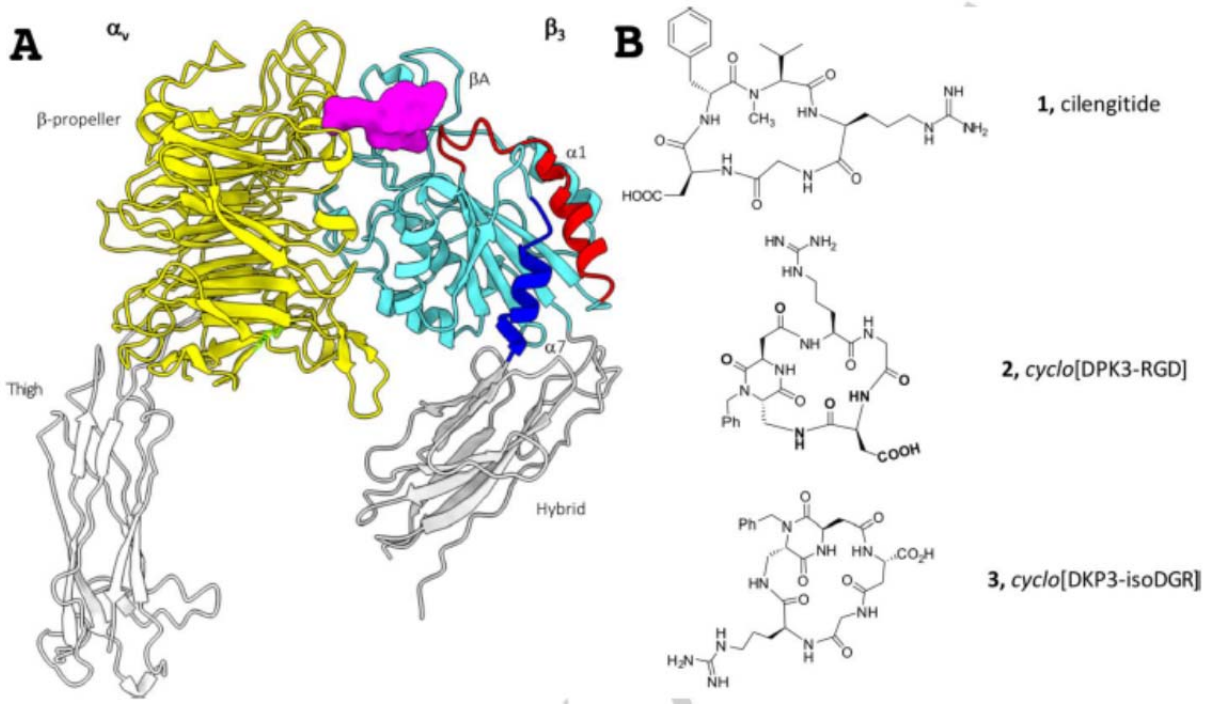

Figure 1. αvβ3 integrin complex. (A) αvβ3 ectodomain representation (for clarity only simulated system is shown). Integrins subunits are displayed in cartoon representation, αv (β-propeller and Thigh) domains are coloured yellow and white, respectively, while β3 (βA and Hybrid) domains are coloured cyan and grey, respectively. The ligand binding site is indicated as magenta solid surface at the αvβ3 interface. α1 and α7 helices of the β3 domain are evidenced and labelled. (B) Peptidomimetics. Integrin ligands are displayed and numbered: 1 = cyclo-RGDf(NMe)V/Cilengitide; 2 = cyclo[DKP3-RGD]; 3 = cyclo[DKP3-isoDGR].

Results and Discussion

Comparative Analysis of Ligand-Dependent Integrin dynamics

Ligand-dependence of β3-domain motions. MD simulations (2 microseconds for each system) have been performed for αvβ3-Cilengitide (Complex **1**), αvβ3-*cyclo*[DKP3-RGD] (Complex **2**), and αvβ3-*cyclo*[DKP3-isoDGR] (Complex **3**). We first set out to analyze the structural features that may be linked to the conformational (de)activation of αvβ3 dynamics. In particular, it has been suggested that the process is primed by structural adjustments that involve substructures of the β3 subdomain, which ultimately determines the extension/opening of the β-hybrid domain. In this framework, the distance between the two β3 subdomains, namely βA and hybrid domains, is taken as an index of opening. In fact, the center of mass (COM) distances of the two domains in the X-ray structures of integrin αIIbβ3 in the close-to-open transition range from 36.2 Å of the 1st (closed) state to 38.9 Å of the 8th (fully open) state.[1d]

In Figure 2, the corresponding distributions of the COM distances of the βA and hybrid subdomains in the calculated structures are reported. The COM distances for the complex with Cilengitide (Complex **1**) show a distribution with two significant peaks, one corresponding to the initial closed conformation (~ 36 Å), the other (at a higher value of ~ 40 Å), indicating the possibility of βA and hybrid domains to sample a significantly more open orientation. Complex **2**, in which the RGD motif is still present but is supported on a diketopiperazine scaffold, shows a significantly less populated open β3 structure. Complex **3** shows the highest propensity for compact states. In general, DKP3-molecules appear to block the opening motion of the β3 subdomain, with compound **2** partially reminiscent of the behavior of compound **1.**

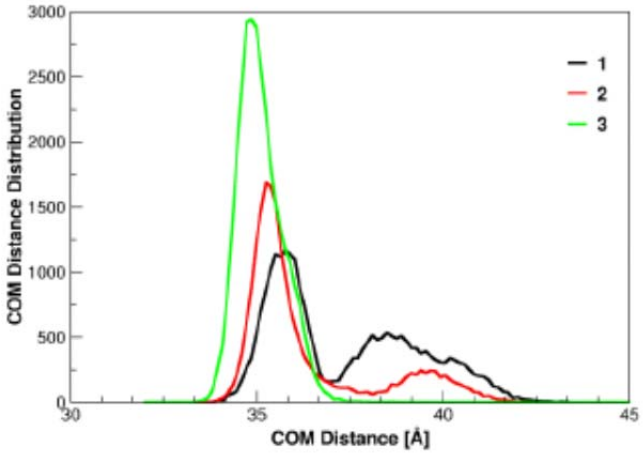

Figure 2. **Center Of Mass distance between βA and hybrid domains.** Histogram reporting on the distribution of the Center Of Mass (COM) distances between the βA and hybrid domains in the β3 subunit of the integrin. The x-axis reports increasing distances between the COMs, while the y-axis reports the number of frames in which a certain distance is realized.

To focus on ligand-induced changes at the residue-level resolution, we characterized residue-flexibility modulation throughout the whole protein by means of local fluctuation (LF) analysis.[15] This calculation informs on the fluctuations of the distances between any pair of residues in the ensemble (*i, i±2*), where *i* is the sequence number, thus highlighting structural deformations that involve contiguous sequence stretches, and highlighting allosteric connections. Ligands recognize and bind RGD-integrins in a groove between αv and β3, engaging both subunits via the electrostatic clamp created by the RGD motif mentioned above. In particular, β1-α1, α2-α3 and α6-α7 loops of the β3 subunit are either directly or indirectly (through metal ions) coordinated by the docked molecule and the nearby helix α7 is considered the key element for initiating the structural rearrangement required by the hybrid domain to swing-out, leading to integrin extension through a piston-like movement.[1d-f] In β3, loop α1-α2 and helix α1 (~ aa. 115-143) in complex **1** correspond to a higher peak indicating higher flexibility with respect to the other complexes (Figure 3). Moreover, residues between 155 and 205 appear differently modulated depending on the ligand. Specifically, with compounds **1** and **2**, α2-α3 loop (~ aa. 210-220) results very flexible, while helix α2 is rigid. Helix α7 (~ aa. 343-351) shows a larger degree of fluctuation

when Cilengitide (compound **1**) is bound. It is interesting to observe that the higher LF for this helix in complex **1** is coupled to a more rigid α6-α7 loop (~ 325-342 aa), compared to the other complexes. The rigidification of the loop facilitates the displacement of the following α7-helix as a rigid-body, which is at the basis of the hybrid domain opening, consistent with the COM distance distribution analysis.

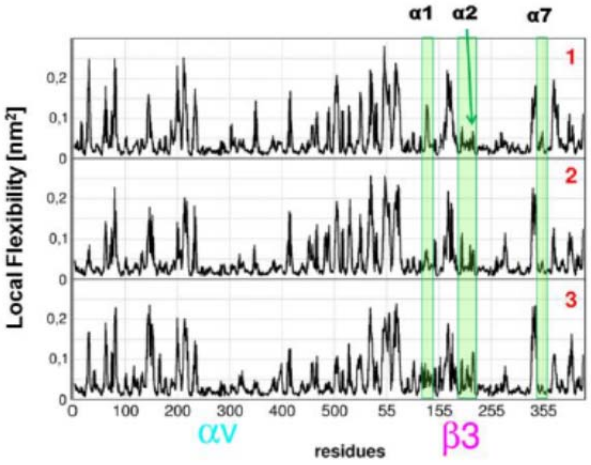

Figure 3. **Local Fluctuations (LF) in the different integrin-ligand complexes.** LF per residue is averaged along the full-length simulation time, indicating how much the average distance of a residue from neighboring residues fluctuates in a simulation. The two subunits are reported along the sequence. The α_V subunit is numbered from 1 to 599 (β-propeller: aa. 1-438, Thigh: aa. 439-599), β_3 from 55 to 435 (βA: aa 109-352, Hybrid: aa. 55-108, 353-434). α1 (133-143), α2 (200-209), α7 (343-351) within the β_3 domain are evidenced with green boxes and labelled. The red numbers in the graphs refer to the different complexes.

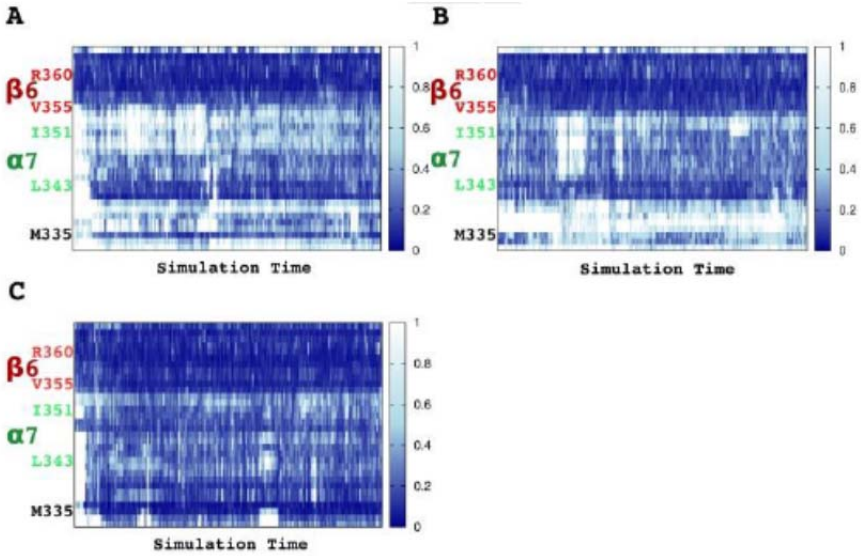

Figure 4. **Time evolution of the geometrical strain calculated for $\beta A_{\beta 3}$ in the different integrin-ligand complexes.** X-axis reports the simulation time of a representative replica per complex **1** (A), complex **2** (B), complex **3** (C); on the y-axis βA sequence is reported and key amino acids are evidenced: Met335 (at the top of the loop preceding α7 and discussed in the main text) and amino acids delimiting helix α7 (LIVDAYGKI) and strand β6 (VELEVR) are labelled.

To further confirm these observations, we set out to calculate the geometric strain (see methods) of the β3-domain.[15c, 16] Strain analysis reports on the deformations of the contact networks of residues. In Figure 4, we plot the comparison between βAβ3 traits of representative replicas of Complexes **1, 2** and **3**, and in particular we draw the geometrical strain evolution of α7 and β6 motifs along the simulation time. From the figure it is clear that the local strain is differentially distributed in Complex **1**, indicating a higher degree of conformational freedom to β3.

We next focus on the dynamics of the whole β3-domain and locally of the α7-helix, considered the key players in priming the opening: Principal Components Analysis (PCA) is used to investigate the slow, large amplitude motions of these

approximately-rigid subparts, which may give distinct responses to the presence of a certain ligand.[17] In Figure 5 the projection of the full-length trajectories for each ligand on the essential space defined by the two principal eigenvectors of the trajectory of Complex **1** (see methods) are plotted. The broadest distributions of the β3 domain and α7-helix pertain to Complex **1**, indicating that the presence of Cilengitide can induce a larger structural variability compared to the other cases. The conformational space spanned by Complex **2** is significantly reduced compared to the previous case. Compound **3** confines β3 and α7 structural variability in a very limited (indeed the most limited one) region of the essential space.

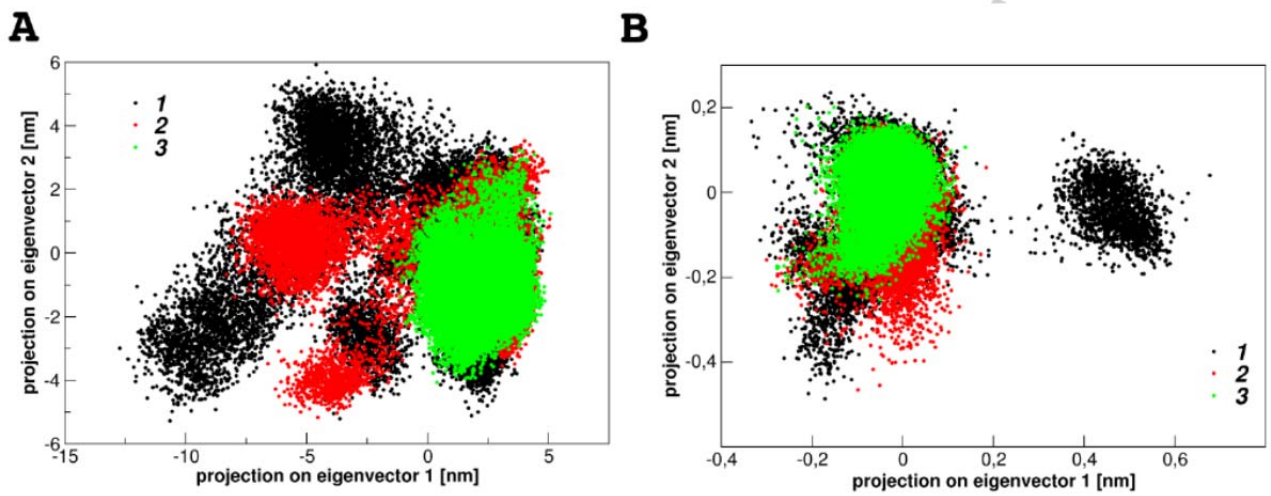

Figure 5. **Principal Components Analysis.** Principal component analysis on (A) β_3 subunit and (B) α7 helix for the three complexes. Cilengitide (compound **1**) covariance matrix has been taken as reference for other compounds trajectory projection. The first two principal components (eigenvectors 1 and 2 on x- and yaxes) are used for the projection, covering 78% (for β_3) and 77% (for α7) of the total variance. Black points are used for compound **1**, red for compound **2**, green for compound **3**.

Evolution of interactions and ligand conformations in the binding pocket. In order to characterize ligand-dependent networks of interactions connected to the selection of specific integrin conformations, we analyzed the evolution/conservation of interactions of the ligands in the binding pocket along the trajectories. In general, except for the carboxylate oxygen of the RGD (or isoDGR) aspartic acid that stably coordinates the metal ion at MIDAS, ligand interactions show a dynamic behavior along the simulation time. Figure S1 shows the full conformational space spanned by the panel of small molecules. Interestingly, Complex **1** is the best example where the compound, Cilengitide, bridges the two chains for a considerable window of the simulation time, exchanging interactions with different charged amino acids onto αv surface (Figures 6, S1-B and Table 1).

Table 1 reports on the H-bonds established at the interface by each compound that are conserved along the simulation time. In Complex **1,** Cilengitide is bound to αv chain via multiple hydrogen bonds, making contacts with either the X-ray residue Asp150αv or Asp148αv, Glu121αv and Glu123αv, while the other Xray interaction with Asp218αv is poorly sampled (about 2%). In the case of compounds **2** and **3**, the electrostatic lock with the β-propelleraν domain is principally mediated by Asp218αv, as in the starting docking poses. Figure 6 shows the interchange among polar residues at the β-propeller that keep Cilengitide at the αv subunit: in particular, the starting bridges with Asp218αv and Asp150αv can be dynamically and reversibly replaced by Asp148αv, Glu121αv and Glu123αv. The high motility of the guanidinium moiety and the capability to establish a set of diverse, yet chemically similar and overall stable interactions by Cilengitide is qualitatively reminiscent of the variable interactions network shown by wtFN in previous studies.[2b] Interestingly, wtFN is known to act as an endogenous partial agonist, as shown experimentally by Van Agthoven and colleagues.[2a]

The interaction common to all ligands is the coordination to Mn2+ at MIDAS. An important contribution is also given by the interaction with Asn215β3 at α2-α3 loop, which plays a crucial role in the stabilization of all compounds. This interaction was previously reported as particularly stable also in wtFN and hFN complexes. [2]

Table 1. Ligand-$\alpha_v\beta_3$ Hydrogen bonds.

Compound	*H bonds (%)*
1	**Y178** (4.3), **E121** (16.6), **E123** (15.5), **D148** (10.9), **D150** (17.2), **D218** (2.2), S123 (13), S121 (1.9), N215 (37.3), R216 (1.9)
2	**Y178** (1.7), **E121** (5.9), **E123** (21.9), **D148** (13.6), **D218** (40.8), **D219** (14.5), S121 (3.9), S123 (43.7), Y166 (1.7), R214 (8.9), N215 (18.9), D217 (1.3)
3	**D218** (35.6), **D219** (14), S121 (22.1), S123 (4.6), N215 (28), D251 (18.1)

Amino acids from the α_v subunit are in bold.

It is worth pointing out that in the starting X-ray structure (1L5G) the ArgRGD side chain of Cilengitide points into a groove at the top of the β-propellerαv domain, where it is held in place by a bidentate salt bridge to Asp218αv at one side and Asp150αv at the other. This coordination favors a large solvent exposure of the upper portion of the ArgRGD side chain.[1b] In the presence of compound **1** (Cilengitide) a set of interactions in dynamic exchange are formed with both subunits (Figure 6). Similarly to wtFN, [2b] new electrostatic interactions are made with β-propellerαv residues (namely, Glu121αv, Glu123αv, Asp148αv). To a smaller degree, compound **2** shifts between similar polar interactions, although the ArgRGD-Asp218αv bond is the most stable. In the complex with compound **3,** the interaction with Asp218αv is the most populated among the αv residues. The exposed character of this part of the guanidinium group is well-conserved in the analysis of the various ligand binding poses and leads to larger fluctuations of the corresponding side chain between the solvent and the binding pocket.

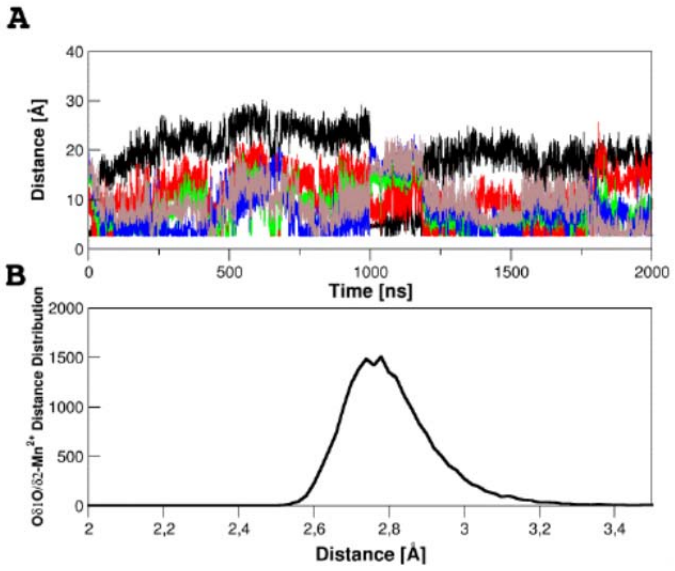

Figure 6. **Compound 1 (Cilengitide) electrostatic clamp.** (A) Time evolution (2 μs) of polar interactions made by Arg_{RGD} and charged residues at the α_v subunit: interaction with $Asp218_{\alpha v}$ is shown in black, $Asp150_{\alpha v}$ in red, $Asp148_{\alpha v}$ in green, $Glu121_{\alpha v}$ in blue, $Glu123_{\alpha v}$ in brown. (B) Distribution of the coordination distance between Oδ1/Oδ2 Asp_{RGD} and Mn_{2+} at MIDAS in Cilengitide complex (1) simulation.

Overall, these results indicate that the guanidinium moiety of the ligands does not appear to be anchored in a specific interaction despite the well-accepted description of the electrostatic clamp. On the contrary, the binding space sampled by all three compounds shows relevant overlap among the carboxyl groups of the Asp substructure of the ligand.

Our results are consistent with the structure-based description of the activation mechanism of the highly-related integrin αIIbβ3. In this context, Zhu *et al.* demonstrated the prominent role of the Asp side chain in determining the opening motion at the basis of the activation mechanism with respect to the Arg basic moiety: herein, while the Arg electron density is weakly resolved from state 1 to 6,[1d] the electron density for Asp is well defined in all the states. In a subsequent paper, the same group demonstrated that AGDV and RGD peptides have analogous affinities for the αIIbβ3

integrin headpiece, showing that AGDV can induce complete headpiece opening in solution and that Lys or Arg residue is not essential for inducing a full headpiece opening in αIIbβ3, whereby “the contributions in binding free energy of the salt bridge and other additional contacts with α are relatively minor when compared to the interactions with β”.[18] Focusing on the ligand structural evolution, the Cβ-Cβ distance of ArgRGD and AspRGD of the tripeptide is homogeneously distributed around 8 Å for compound **1**, while the distance distribution of compounds **2** and **3** shows two main populations corresponding to shorter and larger distances (Figure S2). Further corroborating the observations on interactions with the protein, guanidinium and phenyl groups are flexible on αvβ3 surface, populating also compact structures that still permit the coordination of carboxyl Asp oxygens.

Interface lock: role of FN-like hydrophobic interactions. Previous studies have demonstrated the crucial role of a π-π interaction between integrin Tyr122β3 and high-affinity Fibronectin (hFN) Trp1496 and the consequent formation of a hydrophobic packing between integrin and the endogenous ligand in determining the antagonistic activity of Fibronectin.[1f, 2a] It was shown that the hydrophobic lock at the interface significantly limits structural flexibility of the two domains, thus ‘freezing’ the full β3 integrin dynamics that is required for the opening and activation processes.

In the starting peptidomimetics conformations, aromatic moieties of RGD ligands (compound **2**) overlap with Cilengitide D-Phe side chain of the X-ray complex interacting with Tyr122β3, while the benzyl group of the isoDGR compound (compound **3**) packs with Tyr178αv, Arg214β3 and Tyr166β3 side chains (Figure S3). The hydrophobic cluster described for hFN (antagonist) is composed by Tyr1446-Trp1496 from the ligand (hFN) and Tyr122β3-Trp129β3 from the αvβ3. Within α1, blockage of Tyr122β3 and Trp129β3 reverberates on the near β6-α7 loop, which in turn modulates the mobility of α7.

In the case of the small molecules, the mutual arrangement between the aromatic rings of the cyclopeptides and Tyr122β3/Tyr166β3 can be hypothesized to perform a function equivalent to that of the hydrophobic cluster observed for the Fibronectin domain (hFN).[2a]

To investigate this aspect, we measured the distances between the centroids of the phenyl groups of cyclic RGD peptides and Tyr122β3 on one hand (Figure 7) and between the two phenyls of Tyr122β3 and Tyr166β3 on the other hand (Figure S4). Except for compound **2** that forms a π interaction with Tyr166β3, the other ligands present distributions of Tyr122β3-aromatic distances that are consistent with the presence of a stacking interaction, whereas packing between Tyr122β3 and Tyr166β3 settles at larger yet less variable distance values. Interestingly, Trp129β3 results distant -and flexible- from putative hydrophobic packing induced by the small ligands and its coordination is rather favored by the large endogenous Fibronectin domain.

Examination of the aromatic ring orientation of compound **2** along the simulation time shows that favourable van der Waals interactions can be observed between the benzyl group and Ser123β3, Lys126β3, Ala128β3, Tyr166β3, Met180β3, in agreement with previous NMR-STD data.[19] Compared to starting docking poses, the aromatic group of compound **2** loses the interaction with Tyr122β3 to pack with Tyr166β3, while ligand **3** can form a new π interaction with Tyr122β3.

In this framework and in line with our previous studies, we analyzed specific dynamic changes that take place at the binding site level to shed light on the relationship between ligand features and integrin structural preferences. Indeed, in our previous studies of αvβ3 in complex with wild type and high-affinity Fibronectin, we found that small structural modifications occurring at the RGD-binding pocket can be associated to different steps in integrin activation. Therefore, we monitored the distance between the carbonyl oxygen of Met335β3 and Mn2+ at ADMIDAS, as an indicator of the opening process described for αIIbβ3 and the activation of αvβ3 by Fibronectin. In Figure 8 and Table 2 the relative distributions of such distance is plotted per ligand: larger Met-ADMIDAS distances, recorded for compound **1** and, to a smaller degree, also for compound **2**, are more likely consistent with the opening mechanism already reported and associated to βA allostery.[1b, c, 2a, 20] Starting X-ray distance between the two atoms is 10.8 Å (given as an intermediate distance value between the fully-open state and the closed form [1b, c, 2a, 20]); while compound **3** essentially oscillates around this value, the tail in compound **1** distribution accounts for those Met-ADMIDAS distances that are associated to very compact αvβ3 shapes.

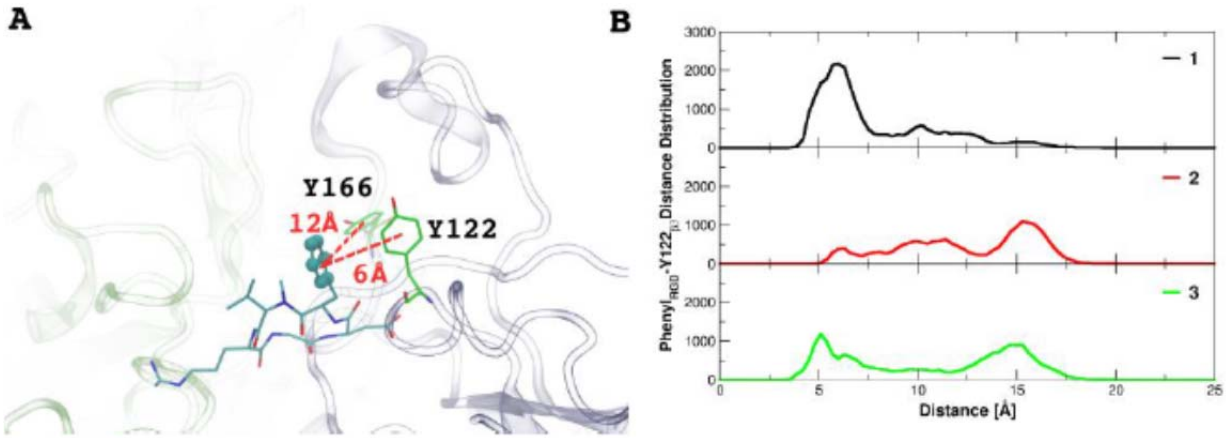

Figure 7. **π-π stacking.** (A) Hydrophobic packing between RGD-ligand phenyl ring and Tyr122$_{\beta3}$ (β1-α1 loop) is indicated on the 3D structural representation.(B) Distance between centroids is given. For comparison RGD-ligand phenyl and Tyr166$_{\beta3}$ is also indicated in A. Black line: compound **1;** red line: compound **2;** green line: compound **3.**

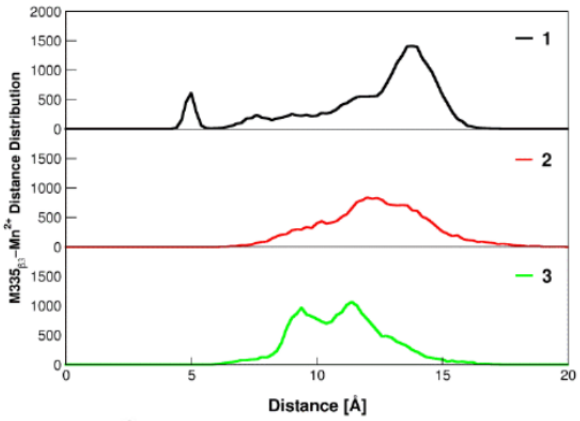

Figure 8. **Met335$_{\beta3}$-Mn$_{2+}$ distance.** Met335$_{\beta3}$ at β6-α7 loop and metal ion at ADMIDAS preferentially sample larger distances in complex with compound **1**; the displacement length gradually decreases from compound **1** to **3**. Distribution details are given in Table 2.

Overall, MD-based data indicate that compound **1,** Cilengitide, induces higher internal flexibility in the integrin favoring dynamic states that can favor transitions to the open state. In contrast, compound **3**, which features the *cyclo*[DKP] scaffold combined to the isoDGR motif appears to lock the integrin in the closed state. Finally, compound **2,** which combines the *cyclo*[DKP] scaffold with the RGD recognition motif characteristic of Cilengitide, shows an intermediate behavior.

Table 2. Mean values of the distance between the carbonyl oxygen of Met335$_{\beta3}$ and Mn$_{2+}$ at ADMIDAS.

Compound	Average (Å)	Median (Å)
1	12.0	12.98
2	12.24	12.20
3	10.87	10.86

Effect of RGD and isoDGR-containing cyclopeptides on αvβ3 conformation on MSR3 melanoma cells. The effects of RGD- and isoDGR-containing cyclopeptides on αvβ3 conformational dynamics have been previously investigated using the monoclonal antibody AP5,[14] a specific antibody capable of recognizing the active form of αvβ3 on the cell surface. In particular, this antibody recognizes a small epitope at the amino terminus of the β3 subunit, the so-called ligand-induced binding site (LIBS), which is hidden in the inactive integrin and is exposed upon agonist binding or partial integrin activation. These studies showed that Cilengitide (compound **1**) and other RGD-based molecules, but not isoDGR cyclic penta- or hexapeptides (e.g. *cyclo*-CGisoDGRG), can induce a significant exposure of the β3-LIBS

epitope on human umbilical vein endothelial cells and MSR3 melanoma cells, as revealed by FACS analysis of cells with mAb AP5.[8c, 10]

Keeping this in mind, in the present work we examined the effects of compounds **2** and **3** (containing the RGD and the isoDGR motif, respectively) on αvβ3 integrin conformation in MSR3 melanoma cells, and compared the results with those obtained with Cilengitide and *cyclo*-CGisoDGRG (called **CTRL** compound, previously studied and not simulated here). Consistent with previous studies, FACS analysis of MSR3 cells with mAb AP5 (Figure 9A) showed that compound **1** (Cilengitide, 50 and 500 μM) could markedly increase antibody binding to the cell surface, pointing to integrin conformational changes (Figure 9B). Consistent with MD observations, compound **2** (*cyclo*[DKP3-RGD], 50 μM and 500 μM), while causing an increase in antibody binding, does so to a smaller degree than Cilengitide (Figure 9B). This suggests that compound **2** could also induce a change in the conformation of the β3 subunit, resulting in a moderate exposure of LIBS.

Notably, none of these peptides could affect the binding of the mAb LM609 (Figure 9C),[8c] an isotype-matched monoclonal antibody capable of recognizing the headpiece region of αvβ3 in all integrin conformational states,[21] data indicating that the effects observed with AP5 were indeed related to conformational changes and not to changes in integrin expression.

In contrast, no effects on antibody binding were observed with *cyclo*-CGisoDGRG or with compound **3** (*cyclo*[DKP3-isoDGR]), even when large excesses of ligands (500 μM) were used (Figure 9B). Thus, also the cyclic peptidomimetic **3**, similar to *cyclo*-CGisoDGRG, did not induce exposure of the β3-LIBS epitope, suggesting that also this peptidomimetic can act as an integrin antagonist, and not as an agonist. These observations fully corroborate computational results, showing that compound **3** blocks the integrin in an inactive dynamic state, and support the concept that the lack of integrin activation and the pure integrin antagonism are general intrinsic properties of the isoDGR motif.[8c]

Conclusions

α_V clamping and conformational rearrangement: a model for integrin (de)activation. The activation process of integrins takes place through a large conformational change that involves mostly β_3 structural rearrangements upon ligand binding at the top of the αβ. The recognition and binding of the two subunits at once has been considered essential to favour the extension of β_3 leg via the separation of βA and hybrid domains.

Experimental binding affinities of compounds **2** and **3** to integrin $\alpha_v\beta_3$, expressed as the concentration of compound required for 50% inhibition of biotinylated vitronectin binding to isolated $\alpha_v\beta_3$ integrin, are comparable to the low nanomolar IC_{50} value of Cilengitide (IC_{50}s of 4.5 and 9 nM for $\alpha_v\beta_3$ for compounds **2** and **3**, respectively),[13, 22] yet their molecular effects on $\alpha_v\beta_3$ conformation on MSR3 cells probed by the binding of mAb AP5, turn out to be different.

From our analyses, all compounds are able to (reversibly) form the electrostatic clamp that binds α_V at one site and β_3 at the other. The compounds show distinct degrees of mobility at the interface: while compound **1** appears associated to a larger conformational variability, compound **2**, chemically similar to **1** in the RGD recognition motif but featuring the DKP scaffold**,** appears to be more stable and less dynamic at the interface. Compound **3** is stable in binding modes at the interface that prevent integrin mobility.

In particular, the comparative analysis of the impact of ligands on the internal dynamic properties of $\alpha_v\beta_3$ show that the COM distances of the βA and hybrid subdomains sample open β_3 conformations in the calculated structures of compound **1** and, to a significantly smaller extent, in those of **2** (Figure 2). In contrast, COM distances that correspond only to closed states are sampled for compound **3**. Principal Components Analysis, used to investigate the dynamics of the whole β_3-domain and locally of the α7-helix, indicates that the presence of Cilengitide induces the largest structural variability among the cases studied (Figure 5), whereas compound **2** and even more **3** confine the protein distribution in a limited region of the conformational space.

The ligand-induced changes at the protein residue-level displayed by the local fluctuation analysis (Figure 3), as well as the strain analysis reporting on the deformations of the contact networks of residues (Figure 4) confirm a higher degree of fluctuation and conformational freedom when Cilengitide is bound with respect to the other complexes.

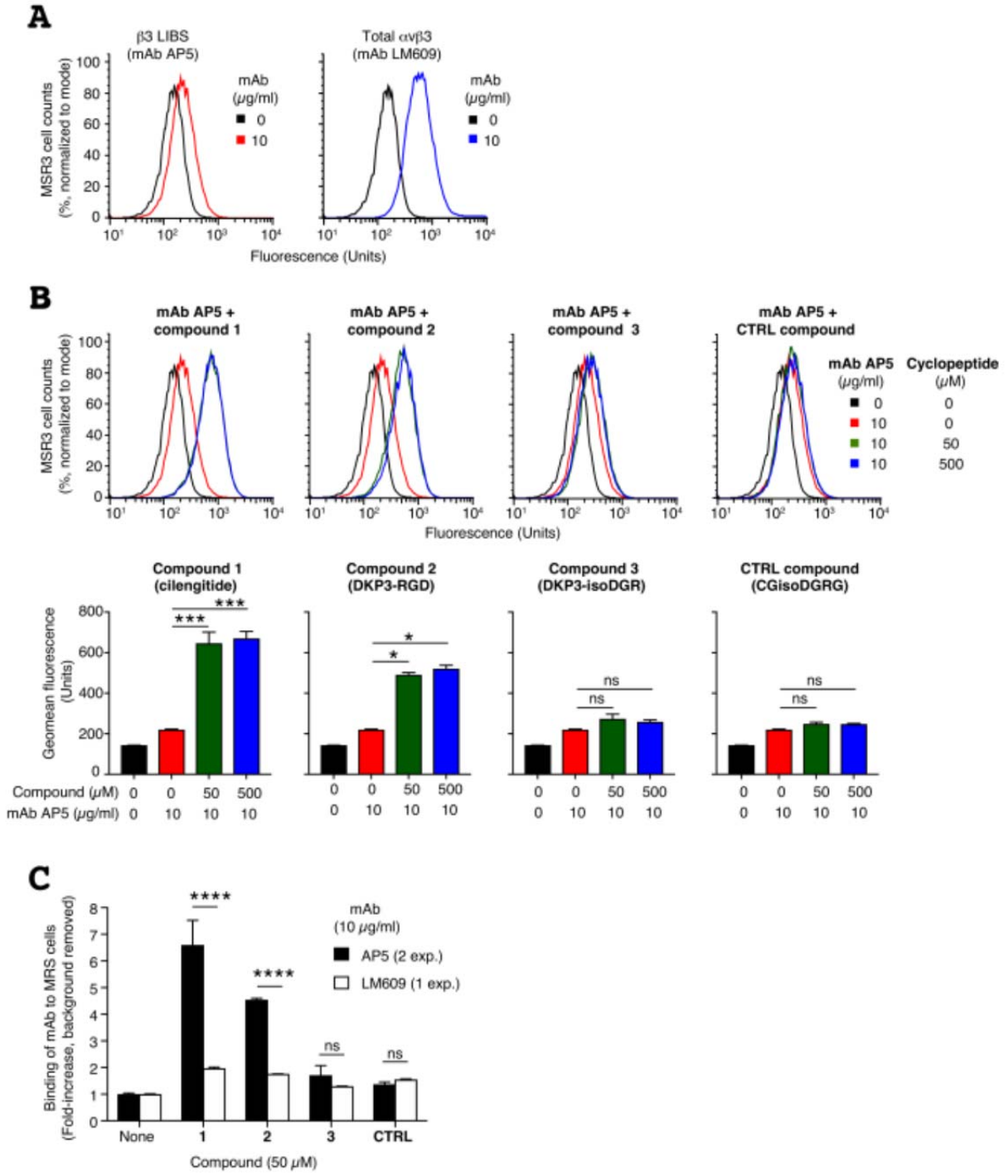

Figure 9. **Effect of compounds containing the RGD or isoDGR motives on $\alpha_v\beta_3$ conformation on MSR3 cells.** (A) $\alpha_v\beta_3$ expression on MSR3 cells as detected by flow cytometry analysis with the anti-β3-LIBS mAb AP5 (against the active conformation, left), and with the mAb LM609 (against the total $\alpha_v\beta_3$, right).(B) Effect of compounds **1**, **2**, **3** and **CTRL** at the indicated concentrations on mAb AP5 binding. Representative flow cytometry analysis (upper panels) and quantification of antibody binding (lower panels). Bars, mean ± SD of two independent experiments in duplicate. ***, P<0.001; *, p<0.05; by Kruskal-Wallis test followed by Dunn's multiple comparisons test. (C) Effects of compounds **1**, **2**, **3** and **CTRL** on mAb AP5 or mAb LM609 binding. Background, refers to the binding of goat anti-mouse Alexa-488 labelled secondary antibody alone. Bar, mean ± SD of the indicated number of independent experiments in duplicate. ****, P<0.0001 by two-way ANOVA followed by Sidak's multiple comparisons test.

In this context, an important question is whether or not the electrostatic clamp for integrin activation is directly linked to the activation mechanism or if it is relevant only to the recognition process.

From our results, the formation of the electrostatic clamp observed in Complex **1** may correlate with the observed activation.[18] This may partly explain the observed agonist behavior of Cilengitide at low concentrations: only in such conditions the enhanced conformational flexibility shown by Cilengitide may favor poses of the electrostatic clamp that promote the formation of interactions required for activation. Stable π-π-stacking interactions are important to modulate

β3 opening/blockage.[2] It is interesting to observe that when both electrostatic interactions on αv and good hydrophobic packing on β3 at the opposite side of the ligand (compound **1**) are formed, protein conformational flexibility is enhanced. The specific structural properties of compounds **2** and **3** favor the stabilization of the interface, with compound **2**, featuring the RGD motif, partially reminiscent of the behavior of Cilengitide. An optimized hydrophobic packing (differentially obtained by compounds **2** and **3**) favors the inactivation of the opening motion. Focusing on the guanidinium moiety, polar interactions are stable and localized, while at the carboxyl AspRGD portion interactions mainly concern α2-α3 loop.

Effects of RGD-peptidomimetics revealed by MD simulations provide a detailed molecular rationale for the conformational changes of integrins observed experimentally by flow cytometry analyses with mAb AP5: the level of conformational activation induced by ligand binding, revealed by AP5 binding, correlates well with the higher mobility displayed by integrin bound to compounds **1** and **2**. On the other hand, compound **3** favors the inhibition mechanism by locking integrin dynamics, thus preventing the conformational switch (Figure 9). Importantly, isoDGR-containing cyclopeptides fail in inducing exposure of the β3-LIBS epitope and do not promote the redistribution of αvβ3 from focal adhesion to the cell periphery, required for cell migration, in contrast to what observed for RGDf(NMe)V (compound **1**). This further supports the hypothesis that isoDGR-containing peptides compete with ligand binding without inducing integrin activation.[10]

As a caveat, one has to consider that the use of plain MD simulations, albeit in different ligand states and run for long timescales, provide the details of the initial steps of liganddependent (de)activation. Considering the complexity and large scale rearrangements involved, it is tempting to suggest that enhanced sampling calculations based on metadynamics [23] or Gaussian Accelerated MD, [24] or multiple-resolution methods[25] may be viable approaches to disentangle the intricacies of ligand-based integrin regulation.

In conclusion, we suggest that the delicate balance between the presence of the electrostatic clamp and the presentation of the hydrophobic regions of the ligands into the integrin binding pocket selects the dynamic states of the protein that favor opening vs. closing motions: in this model, docking of the ligand is mainly directed by the electrostatic factors, while the crosstalk between the two integrin subunits is modulated by hydrophobic lock at the top of βA. On these bases, we have rationalized the observed pure antagonist behavior of compound **3** versus the agonist behavior of compound **1.** These results are consistent with previous observations obtained via X-ray analysis and MD simulations on αvβ3-Fibronectin complexes: [2] importantly, here we show that small molecules can recapitulate the integrin modulation mechanisms of endogenous protein ligands and their mutants. This is noteworthy because dynamics-based approaches such as the ones presented here could have implications for drug design: in this framework, the development of optimized integrin blockers could in fact exploit the definition of the roles of different chemical determinants in integrin binding and activation/deactivation to build pharmacophore models to explore new regions of the chemical space and/or guide the development of multivalent/multitargeted systems.[26] The results presented here thus open the possibility to expand the molecular diversity space of integrin agonists and antagonists.

Experimental Section

Docking of DKP ligands. Computational models for the interaction of RGD and isoDGR peptidomimetic ligands (compounds **2**, **3**) with the αvβ3 integrin were built using our previously developed docking approach [27], starting from the X-ray structure of the extracellular segment of integrin αvβ3 complexed with the cyclic pentapeptide ligand Cilengitide (Protein Data Bank entry 1L5G). [1b]

The RGD tripeptide adopts a highly extended conformation across the αvβ3 integrin intersubunit interface. The Arg and Asp side chains extend in opposite directions, and the backbone in between is also extended and characterized by Cβ(Asp)-Cβ(Arg) of 8.9 Å. Docking calculations were performed starting from the macrocycle conformations of the DKP ligands previously reported [12, 27] using Glide version 5.7 (Schrödinger, LLC, New York, NY). [28]

The nanomolar affinity of diketopiperazine-derived cyclic peptidomimetics for the integrin αvβ3 receptor can be attributed to their high structural preorganization. Compared to X-ray RGD bound conformation, all macrocycle geometries display an extended arrangement of the RGD sequence satisfying the pharmacophoric requirements for the binding to integrin αvβ3. In fact, as already reported, [12, 27] docking calculations produced top-ranked poses conserving all the important interactions of the X-ray complex.

In the docking poses, the aromatic moieties of RGD ligands containing the DKP3 scaffold well-overlaid to Cilengitide D-Phe side chain orientation in the crystallographic complex, while the isoDGR compound explores a different protein region by placing the benzyl group between Tyr178αv and Arg214β3, Tyr166β3 side chains.

Docking best poses of each compound were selected as input structures for MD simulations of ligand-protein complexes.

Ligands preparations for MD
The Antechamber program of Ambertools 1.5 was used to generate ligand input file using GAFF force field [29] and RESP charges derived from *ab initio* single point calculation using Gaussian09 [30] (HF, 6-31g*) on the docking best pose. All compounds were considered in their zwitterionic form.
MD settings
Molecular dynamics simulations were carried out on the complexes described before. The starting X-ray model was retrieved from Protein Data Bank with access number 1L5G, where αvβ3 integrin ectodomain is solved in complex with the Cilengitide (compound **1**). The integrin extracellular domain was cut at the Thigh domain of the αv, including β-propeller and Thigh domains (residues 1-599) and at the β-hybrid domain of the β3, including βA and hybrid domains (residues 55-434). For MD simulations results on wtFN and hFN refer to ref. Paladino *et al.*[2b]
Crystallographic Mn2+ ions are conserved at the three integrin metal ion binding sites as well as at the β-propeller domain. The Mn(II) parameters were derived by Ghitti et al.[10] As stated by the authors, 'the computed Mn2+ ion parameters improved the agreement with the experimental data consisting in absolute hydration free energy value and structural properties derived from X-ray scattering or QM/MM calculations'. The MD simulation package Amber v12 was used to perform computer simulation applying Amber-ff99SB*IIdn force field.[31] The two systems were solvated, in a simulation box of explicit water molecules (TIP3P model),[32] counter ions were added to neutralize the system and periodic boundary conditions imposed in the three dimensions. Mn2+ ions were modeled based on hydration free energy parametrization derived from Musco *et al.*[10] Final simulated systems are made of ~ 160 000 atoms. After minimization, systems were subjected to an equilibration phase where water molecules and protein heavy atoms were position-restrained, then unrestrained systems were simulated for a total of 6 microseconds, in a NPT ensemble; Langevin equilibration scheme and Berendsen thermostat[33] were used to keep constant temperature (300 K) and pressure (1 atm), respectively. The Berendsen thermostat was used for the sake of consistency in the comparison with previously reported
simulations.[2b] Moreover, here, we are not interested in accurately calculating thermodynamic properties, but rather to investigate the onset of dynamic changes. Electrostatic forces were evaluated by Particle Mesh Ewald method[34] and Lennard-Jones forces by a cut-off of 8 Å. All bonds involving hydrogen atoms were constrained using the SHAKE algorithm.[35] To enhance sampling four independent replicas of 500 ns (4*0.5 μs = 2 μs) were run for each system with different initial velocities. Figures are rendered using VMD,[36] Pymol. [37]
Center Of Mass (COM) distances analysis
Distance length evolution between the two β3 subdomains centroids were analysed by VMD,[36] tools package. Centroids were defined as the center of mass of βA domain (amino acids 109-352) and Hybrid domain (amino acids 55-108 and 353-434). The distance between the two obtained geometric centers was calculated along simulation time for the three complexes.
Local distance fluctuation analysis
We computed distance fluctuations, DF*ij* , along simulations to assess the intrinsic flexibility of proteins. Given r*ij* the distance between Cα atoms of residues i and j : DF*ij* = <(r*ij* − <r*ij*>)2>
distance fluctuation, DF*ij*, is defined as the time-dependent mean square fluctuation of the distance rij , where the brackets indicate the time-average over the trajectory. DF is calculated for any pair of Cα along simulation time. Low DF values indicate highly coordinated residues. LF is the local DF*ij* value averaged among 4 sequential residues (*i*; *j*±2) [16a,38].
Collective motions analysis
Based on the assumption that the major collective modes of fluctuation could be linked to protein function (Essential Dynamics),[17] MD simulations have been analysed by means of principal components analysis (PCA). This method recovers the modes that produce the greatest contributions to the atomic root mean square deviations in the given dynamic ensemble. Thus large-scale collective motions can be collected, as well as the extreme conformations of the system along the simulation, providing information of time-dependent transitions.
Flow cytometry analysis
Flow cytometry analysis of αvβ3 integrin was carried out as described previously.[8b] Briefly, human melanoma MSR3 cells were detached, washed and resuspended with Dulbecco's Phosphate Buffered Saline (DPBS with Ca2+ and Mg2+) containing 1% FCS (binding buffer) in presence of RGD or isoDGR containing compounds (0, 50 or 500 μM), and one of the following antibodies: LM609 (10 μg/ml) and AP5 (10 μg/ml), for 90 min in ice (3x105 cells/100 μl in binding buffer). After washing, the cells were incubated with a goat anti-mouse Alexa488-conjugated secondary antibody (10 μg/ml in binding buffer) for 30 min in ice. After washing, cells were fixed with 4% formaldehyde in DPBS and analysed by flow cytometry.

Acknowledgements

This work was supported by Associazione Italiana Ricerca sul Cancro IG 20019 to GC. The authors would like to thank Dr. Giovanna Musco for discussions and support.

Keywords: integrin • MD simulation • peptidomimetics •conformational changes • flow cytometry analysis

References

[1] a) J.-P. Xiong, T. Stehle, B. Diefenbach, R. Zhang, D. L. Scott, A. Joachimiak, S. L. Goodman and M. Amin, *Science* **2001**, *294*, 339-345; b) J.-P. Xiong, T. Stehle, R. Zhang, A. Joachimiak, M. Frech, S. L. Goodman and M. A. Arnaout, *Science (New York, N.Y.)* **2002**, *296*, 151-155; c) B. D. Adair, J.-P. Xiong, C. Maddock, S. L. Goodman, M. A. Arnaout and M. Yeager, *The Journal of cell biology* **2005**, *168*, 1109-1118; d) J. Zhu, J. Zhu and T. A. Springer, *The Journal of cell biology* **2013**, *201*, 1053-1068; e) J. Takagi, B. M. Petre, T. Walz and T. A. Springer, *Cell* **2002**, *110*, 599-611; f) T. Xiao, J. Takagi, B. S. Coller, J.-H. Wang and T. A. Springer, *Nature* **2004**, *432*, 59-67.
[2] a) J. F. Van Agthoven, J.-P. Xiong, J. L. Alonso, X. Rui, B. D. Adair, S.L. Goodman and M. A. Arnaout, *Nature Structural & Molecular Biology* **2014**, *21*, 383-390; b) A. Paladino, M. Civera, L. Belvisi and G. Colombo, *PLOS Computational Biology* **2017**, *13*, e1005334.
[3] M. Paolillo and S. Schinelli, *Cancers* **2017**, *9*.
[4] a) M. A. Dechantsreiter, E. Planker, B. Mathä, E. Lohof, G. Hölzemann, A. Jonczyk, S. L. Goodman and H. Kessler, *Journal of Medicinal Chemistry* **1999**, *42*, 3033-3040; b) C. Mas-Moruno, F. Rechenmacher and H. Kessler, *Anti-cancer agents in medicinal chemistry* **2010**, *10*, 753-768.
[5] a) G. C. Alghisi, L. Ponsonnet and C. Rüegg, *PLoS ONE* **2009**, *4*; e4449; b) R. E. Nisato, J. C. Tille, A. Jonczyk, S. L. Goodman and M. S. Pepper, *Angiogenesis* **2003**, *6*, 105-119; c) M. A. Buerkle, S. A. Pahernik, A. Sutter, A. Jonczyk, K. Messmer and M. Dellian, *British Journal of Cancer* **2002**, *86*, 788-795; d) S. Yamada, X. Y. Bu, V. Khankaldyyan, I. Gonzales-Gomez, J. G. McComb and W. E.

Laug, *Neurosurgery* **2006**, *59*, 1304-1312; e) S. Loges, M. Butzal, J. Otten, M. Schweizer, U. Fischer, C. Bokemeyer, D. K. Hossfeld, G. Schuch and W. Fiedler, *Biochemical and Biophysical Research Communications* **2007**, *357*, 1016-1020.
[6] R. J. D. Hatley, S. J. F. Macdonald, R. J. Slack, J. Le, S. B. Ludbrook and P. T. Lukey, *Angewandte Chemie - International Edition* **2018**, *57*, 3298-3321.
[7] A. R. Reynolds, I. R. Hart, A. R. Watson, J. C. Welti, R. G. Silva, S. D. Robinson, G. Da Violante, M. Gourlaouen, M. Salih, M. C. Jones, D. T. Jones, G. Saunders, V. Kostourou, F. Perron-Sierra, J. C. Norman, G. C. Tucker and K. M. Hodivala-Dilke, *Nature Medicine* **2009**, *15*, 392-400.
[8] a) L. Marinelli, A. Lavecchia, K.-E. Gottschalk, E. Novellino and H. Kessler, *Journal of Medicinal Chemistry* **2003**, *46*, 4393-4404; b) F. Nardelli, C. Paissoni, G. Quilici, A. Gori, C. Traversari, B. Valentinis, A. Sacchi, A. Corti, F. Curnis, M. Ghitti and G. Musco, *Journal of Medicinal Chemistry* **2018**, *61*, 7474-7485; c) A. O. Frank, E. Otto, C. Mas-Moruno, H. B. Schiller, L. Marinelli, S. Cosconati, A. Bochen, D. Vossmeyer, G. Zahn, R. Stragies, E. Novellino and H. Kessler, *Angewandte Chemie International Edition* **2010**, *49*, 9278-9281.
[9] a) F. Curnis, A. Sacchi, A. Gasparri, R. Longhi, A. Bachi, C. Doglioni, C. Bordignon, C. Traversari, G.-P. Rizzardi and A. Corti, *Cancer Research* **2008**, *68*, 7073; b) A. Corti and F. Curnis, *Journal of Cell Science* **2011**, *124*, 515.
[10] M. Ghitti, A. Spitaleri, B. Valentinis, S. Mari, C. Asperti, C. Traversari, G.P. Rizzardi and G. Musco, *Angewandte Chemie - International Edition* **2012**, *51*, 7702-7705.
[11] A. Felline, M. Ghitti, G. Musco and F. Fanelli, *Biochimica et Biophysica Acta (BBA) - General Subjects* **2017**, *1861*, 2367-2381.
[12] M. Mingozzi, A. Dal Corso, M. Marchini, I. Guzzetti, M. Civera, U. Piarulli, D. Arosio, L. Belvisi, D. Potenza, L. Pignataro and C. Gennari, *Chemistry (Weinheim an der Bergstrasse, Germany)* **2013**, *19*, 3563-3567.
[13] S. Panzeri, S. Zanella, D. Arosio, L. Vahdati, A. Dal Corso, L. Pignataro, M. Paolillo, S. Schinelli, L. Belvisi, C. Gennari and U. Piarulli, *Chemistry - A European Journal* **2015**, *21*, 6265-6271.
[14] S. Honda, Y. Tomiyama, A. J. Pelletier, D. Annis, Y. Honda, Orchekowski, Z. Ruggeri and T. J. Kunicki in *Topography of Ligandinduced Binding Sites, Includind a Novel Cation-sensitive Epitope (AP5) at the Amino Terminus, of the Human Integrin β3 Subunit*, *Vol.* **1995**, pp. 11947-11954.
[15] a) F. Chiappori, I. Merelli, G. Colombo, L. Milanesi and G. Morra, *Plos Computational Biology* **2012**, *8*, e1002844; b) E. Moroni, D. A. Agard and G. Colombo, *Journal of Chemical Theory and Computation* **2018**, *14*, 1033-1044; c) G. Morra, R. Potestio, C. Micheletti and G. Colombo, *PLoS Computational Biology* **2012**, *8*, e1002433.
[16] a) M. Ferraro, I. D'Annessa, E. Moroni, G. Morra, A. Paladino, S. Rinaldi, F. Compostella and G. Colombo, *Journal of Medicinal Chemistry* **2019,** *62,* 60-87; b) R. Potestio, F. Pontiggia and C. Micheletti, *Biophys J.* **2009**, *96* 4993-5002 ; c) F. Pontiggia, A. Zen and C. Micheletti, *Biophys J.* **2008**, *95* 5901-5912.
[17] a) A. Amadei, A. B. M. Linssen and H. J. C. Berendsen, *Proteins: Structure, Function and Genetics* **1993**, *17*, 412-425; b) A. E. Garcia, *Phys. Rev. Lett.* **1992**, *68*, 2696-2699.
[18] F. Y. Lin, J. Zhu, E. T. Eng, N. E. Hudson and T. A. Springer, *Journal of Biological Chemistry* **2016**, *291*, 4537-4546.
[19] I. Guzzetti, M. Civera, F. Vasile, E. M. Araldi, L. Belvisi, C. Gennari, D. Potenza, R. Fanelli and U. Piarulli, *Organic & Biomolecular Chemistry* **2013**, *11*, 3886.
[20] J.-P. Xiong, B. Mahalingham, J. L. Alonso, L. A. Borrelli, X. Rui, S. Anand, B. T. Hyman, T. Rysiok, D. Müller-Pompalla, S. L. Goodman and M. A. Arnaout, *The Journal of cell biology* **2009**, *186*, 589-600.
[21] A. J. Borst, Z. M. James, W. N. Zagotta, M. Ginsberg, F. A. Rey, F. DiMaio, M. Backovic and D. Veesler, *Structure* **2017**, *25*, 1732-1739.e1735.
[22] M. Civera, D. Arosio, F. Bonato, L. Manzoni, L. Pignataro, S. Zanella, C. Gennari, U. Piarulli and L. Belvisi, *Cancers* **2017**, *9*, 128.
[23] a) A. Laio and F. L. Gervasio, *Reports on Progress in Physics* **2008**, *71*, 126601; b) J. Zhu, J. Zhu, A. Negri, D. Provasi, M. Filizola, B. S. Coller and T. A. Springer, *Blood* **2010**, *116*, 5050.
[24] Y. Miao, W. Sinko, L. Pierce, D. Bucher, R. C. Walker and J. A. McCammon, *J. Chem. Theory Comput.* **2014**, *10*, 2677–2689.
[25] a) G. M. S. De Mori, C. Micheletti and G. Colombo, J. Phys. Chem. B 2004, 108, 12267-12270; b) L. Monticelli, D. P. Tieleman and G. Colombo, *The Journal of Physical Chemistry B* **2005**, *109*, 20064-20067; c) M. Neri, C. Anselmi, M. Cascella, A. Maritan and P. Carloni, *Phys. Rev. Lett.* **2005**, *95*, 218102; d) P. Sherwood, B. R. Brooks and M. S. P. Sansom, *Current Opinion in Structural Biology* **2008**, *18*, 630-640.
[26] a) L. Legnani, F. Compostella, F. Sansone and L. Toma, *Journal of Organic Chemistry* **2015**, *80*, 7412-7418; b) F. Compostella, O. Pitirollo, A. Silvestri and L. Polito, *Beilstein J. Org. Chem*. **2017**, *13*, 1008-1021; c) H. M. Sheldrake and L. H. Patterson, Journal of Medicinal Chemistry 2014, 57, 6301-6315; d) A. Sartori, E. Portioli, L. Battistini, L. Calorini, A. Pupi, F. Vacondio, D. Arosio, F. Bianchini and F. Zanardi, *Journal of Medicinal Chemistry* **2017**, *60*, 248-262.
[27] a) A. S. M. da Ressurreição, A. Vidu, M. Civera, L. Belvisi, D. Potenza, L. Manzoni, S. Ongeri, C. Gennari and U. Piarulli, *Chemistry – A European Journal* **2009**, *15*, 12184-12188; b) M. Marchini, M. Mingozzi, R. Colombo, I. Guzzetti, L. Belvisi, F. Vasile, D. Potenza, U. Piarulli, D. Arosio and C. Gennari, *Chemistry - A European Journal* **2012,** *18,*:6195-207.
[28] a) R. A. Friesner, J. L. Banks, R. B. Murphy, T. A. Halgren, J. J. Klicic, D. T. Mainz, M. P. Repasky, E. H. Knoll, M. Shelley, J. K. Perry, D. E. Shaw, P. Francis and P. S. Shenkin, *Journal of Medicinal Chemistry* **2004**, *47*, 1739-1749; b) R. A. Friesner, R. B. Murphy, M. P. Repasky, L. L. Frye, J. R. Greenwood, T. A. Halgren, P. C. Sanschagrin and D. T. Mainz, *Journal of Medicinal Chemistry* **2006**, *49*, 6177-6196.
[29] J. M. Wang, R. M. Wolf, J. W. Caldwell, P. A. Kollman and D. A. Case, *J. Comput. Chem.* **2004**, *25*, 1157–1174.
[30] M. J. Frisch, G. W. Trucks, H. B. Schlegel, G. E. Scuseria, M. A. Robb, J. R. Cheeseman, G. Scalmani, V. Barone, B. Mennucci, G. A. Petersson, H. Nakatsuji, M. Caricato, X. Li, H. P. Hratchian, A. F. Izmaylov, J. Bloino, G. Zheng, J. L. Sonnenberg, M. Hada, M. Ehara, K. Toyota, R. Fukuda, J. Hasegawa, M. Ishida, T. Nakajima, Y. Honda, O. Kitao, H. Nakai, T. Vreven, J. A. Montgomery, J. E. Peralta, F. Ogliaro, M. Bearpark, J. J. Heyd, E. Brothers, K. N. Kudin, V. N. Staroverov, R. Kobayashi, J. Normand, K. Raghavachari, A. Rendell, J. C. Burant, S. S. Iyengar, J. Tomasi, M. Cossi, N. Rega, J. M. Millam, M. Klene, J. E. Knox, J. B. Cross, V. Bakken, C. Adamo, J. Jaramillo, R. Gomperts, R. E. Stratmann, O. Yazyev, A. J. Austin, R. Cammi, C. Pomelli, J. W. Ochterski, R. L. Martin, K. Morokuma, V. G. Zakrzewski, G. A. Voth, P. Salvador, J. J. Dannenberg, S. Dapprich, A. D. Daniels, Farkas, J. B. Foresman, J. V. Ortiz, J. Cioslowski and D. J. Fox in *Gaussian 09, Revision B.01*, **2009**.
[31] K. Lindorff-Larsen, S. Piana, K. Palmo, P. Maragakis, J. L. Klepeis, R.O. Dror and D. E. Shaw, *Proteins* **2010**, *78*, 1950-1958.
[32] W. L. Jorgensen, J. Chandrasekhar, J. D. Madura, R. W. Impey and M.L. Klein, *The Journal of Chemical Physics* **1983**, *79*, 926.
[33] H. J. C. Berendsen, J. P. M. Postma, W. F. van Gunsteren, A. Di Nola and J. R. Haak, *J. Chem. Phys.* **1984**, *81*, 3684-3690.
[34] T. Darden, D. York and L. Pedersen, *Journal of Chemical Physics* **1993**, *98*, 10089-10092.
[35] J. P. Ryckaert, G. Ciccotti and H. J. C. Berendsen, *Journal of Computational Physics* **1977**, *23*, 327-341.
[36] W. Humphrey, A. Dalke and K. Schulten, *journal of molecular graphics* **1996**, *14*, 33-38.
[37] W. L DeLano, **2002**. The PyMOL Molecular Graphics System, Version 2.0 Schrödinger, LLC.
[38] a) A. Paladino, G. Morra and G. Colombo, *J Chem Inf Model* **2015**, *55*, 1377-1387; b) A. Paladino, F. Marchetti, L. Ponzoni and G. Colombo, *Journal of Chemical Theory and Computation* **2018**, *14*, 1059-1070.